Contract No:

This document was prepared in conjunction with work accomplished under Contract No. DE-AC09-08SR22470 with the U.S. Department of Energy.

Disclaimer:

TRANSMISSION ELECTRON MICROSCOPY STUDY OF HELIUM-BEARING FUSION WELDS

M. H. Tosten and M. J. Morgan
Savannah River National Laboratory
Aiken, SC 29808 USA

ABSTRACT

A transmission electron microscopy (TEM) study was conducted to characterize the helium bubble distributions in tritium-charged-and-aged 304L and 21Cr-6Ni-9Mn stainless steel fusion welds containing approximately 150 appm helium-3. TEM foils were prepared from C-shaped fracture toughness test specimens containing delta (δ) ferrite levels ranging from 4 to 33 volume percent. The weld microstructures in the low ferrite welds consisted mostly of austenite and discontinuous, skeletal δ ferrite. In welds with higher levels of δ ferrite, the ferrite was more continuous and, in some areas of the 33 volume percent sample, was the matrix/majority phase. The helium bubble microstructures observed were similar in all samples. Bubbles were found in the austenite but not in the δ ferrite. In the austenite, bubbles had nucleated homogeneously in the grain interiors and heterogeneously on dislocations. Bubbles were not found on any austenite/austenite grain boundaries or at the austenite/δ ferrite interphase interfaces. Bubbles were not observed in the δ ferrite because of the combined effects of the low solubility and rapid diffusion of tritium through the δ ferrite which limited the amount of helium present to form visible bubbles.

INTRODUCTION

Research studies at the Savannah River Site (SRS) have focused on the effects of tritium and its decay product, helium-3, on the mechanical properties of austenitic stainless steels used to contain tritium gas [e.g., 1-3]. These studies have shown that the presence of tritium and helium-3 have a detrimental effect on the fracture toughness properties of these materials. Until recently, studies have focused mainly on the mechanical property variations that occur in the austenitic base materials. However, little work has been done to understand how tritium and helium-3 affect the mechanical properties of the fusion welds that are inherent to the design of some tritium storage vessels.

Typical fusion welds contain austenite (fcc phase) and a smaller amount of δ ferrite (bcc phase). The δ ferrite phase is needed to prevent solidification and

liquation cracking when welding austenitic stainless steels. A recent study of tritium-free material showed that the microstructures that developed in multi-pass fusion welds are very complex and become increasingly so as the δ ferrite content increases [4]. Of prime interest in tritium/helium-containing welds is the role that δ ferrite plays in the deformation/fracture process and how the presence of this phase affects the helium bubble microstructure in the fusion zones.

The purpose of this study was to document the helium bubble distribution that existed in fusion welds made on 304L and 21Cr-6Ni-9Mn stainless steels. This study provided a foundation for understanding the influence of weld microstructure on the helium bubble distribution (size and location) in both the heat-affected zones (HAZs) and fusion zones of these welds.

EXPERIMENTAL PROCEDURE

A series of tritium-charged-and-aged fusion welds, with a range of δ ferrite contents, were prepared using 304L and 21Cr-6Ni-9Mn stainless steel base materials in combination with electron beam and gas tungsten arc welding using a variety of stainless steel filler wires. The base materials were a 304L weld critical plate, a 304L cylindrical forging and a 21Cr-6Ni-9Mn cylindrical forging. The 304L forging was prepared using a high-energy-rate-forging (HERF) process while the 21Cr-6Ni-9Mn forging was made by a conventional forging process. Ferrite levels in the welds varied from about 4 to 33 vol.%. The higher ferrite welds were made using Type 308L, 309L MOD (modified for higher ferrite content), and 312 MOD stainless steel filler wires.

Once welded, the base materials (plate and forgings) were sectioned into C-shaped fracture toughness specimens (Fig. 1). These specimens were exposed to tritium gas at a temperature of 623K and a pressure of about 34 MPa for 3 weeks. The conditions of the charging were designed to saturate the samples with tritium without changing the starting microstructure. After charging, samples were aged for 8 months at 250K to produce a helium content of ~150 appm. Measured helium concentrations in the base metals agreed well with the calculated, target helium concentrations; however, weldments had 33-50% less helium than expected.

Specimens for TEM analysis were prepared from C-shaped specimens after fracture toughness testing. Figure 2 is a schematic illustration of the sample sectioning procedure. Several thin slices were cut from each test specimen beginning immediately adjacent to the fracture surface (plastically deformed region) and continuing into the weld HAZ and base metal. Two 3 mm diameter disks were punched from each slice. Thin foils were prepared from each disk using a twin jet electropolisher and a solution of 57% methanol, 39% butyl cellosolve, and 4% perchloric acid at 35Vdc and 243K. All TEM was performed using a JEOL 2010 operating at 200 kV.

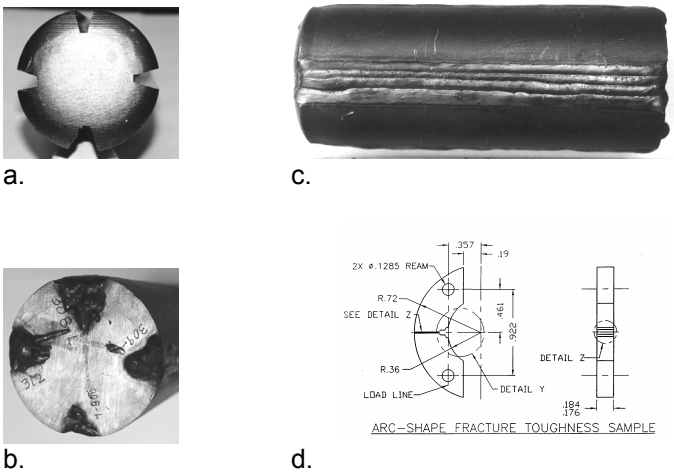

Figure 1. HERF 304L forging showing (a) V-grooves prior to welding, (b) a cross-section of forging after welding, (c) one multi-pass weld along the 8" length of the same forging, and (d) a schematic of a fracture toughness specimen machined from the forgings and weld critical plate. Specimens were machined so the notch would be located at the weld center line.

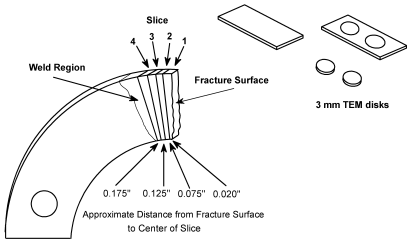

Figure 2. Schematic diagram illustrating the sectioning procedure used to generate TEM disks from the fusion weld region of a fracture toughness specimen.

RESULTS: General Microstructure

Welds with a range of δ ferrite contents of 4 to 33 vol.% were examined in this study. Images shown in Figs. 3a-d illustrate the variety of microstructures observed in the weld fusion zones. Figures 3a-c show the morphological differences in the δ ferrite phase as the volume fraction and Cr_{eq}/Ni_{eq} ratios in the weldments increased. Figure 3d is an image from a low δ ferrite-containing weld that was located close to the fracture surface of a C-shaped

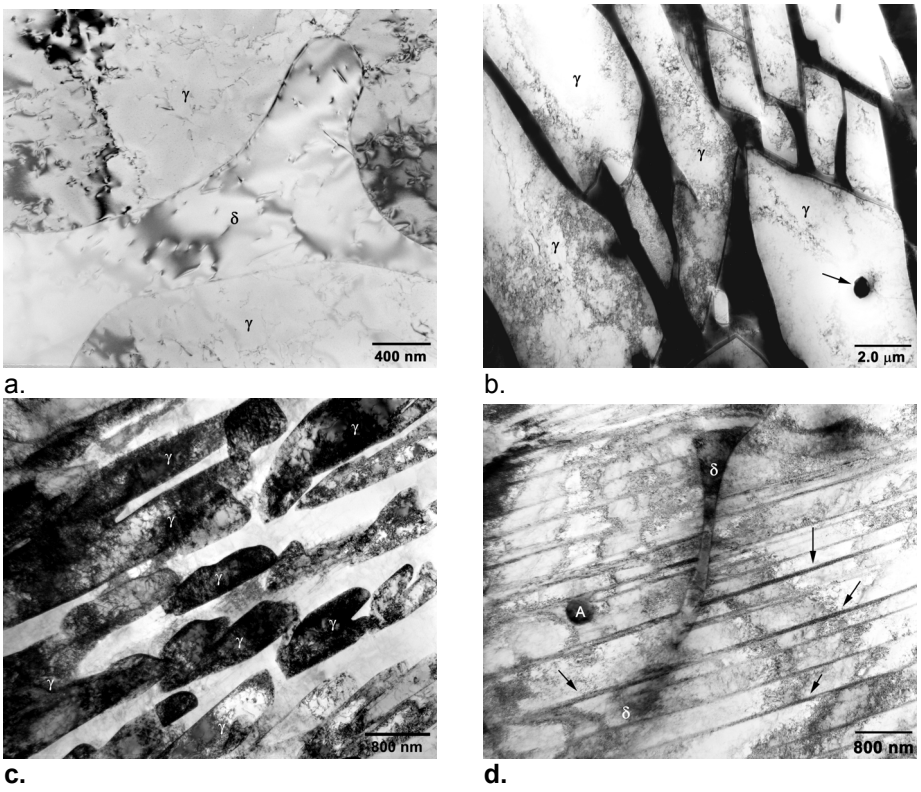

Figure 3. Images of weld microstructures observed in an (a) 8 vol.% δ ferrite weld, (b) a 12 vol.% δ ferrite weld, and (c) a 33 vol.% δ ferrite weld. (d) Deformation twinning in the plastically deformed region of a 5 vol.% δ ferrite weld. Oxide inclusions are located at the arrow in (b) and at "A" in (d).

test specimen. This image shows a microstructure that is mostly austenite with some skeletal ferrite. The more distinctive features in this image, however, are the deformation twins (e.g., marked with arrows) in the austenite. Plastic deformation by way of twinning was observed in all welds in regions closest to the fracture surfaces of the test specimens. Delta ferrite appeared to provide some resistance to deformation, particularly in specimens with higher Cr_{eq}/Ni_{eq} ratios.

RESULTS: Helium-Bearing Welds

The helium bubble distribution in all welds was very similar. Specifically, helium bubbles were observed in the austenite but not in the δ ferrite. Figure 4 is an image from a weld made on the 21Cr-6Ni-9Mn conventional forging using 308L filler wire. This image shows a δ ferrite "grain" in an austenite matrix. The small black "dots" visible in the austenite matrix arise from strain

contrast associated with the presence of helium bubbles. As evidenced in Fig. 4, black "dots" (bubbles) are not present in the δ ferrite. Careful examination of many ferrite regions under a variety of tilt/contrast conditions failed to locate any bubbles in the δ ferrite phase in any of the welds.

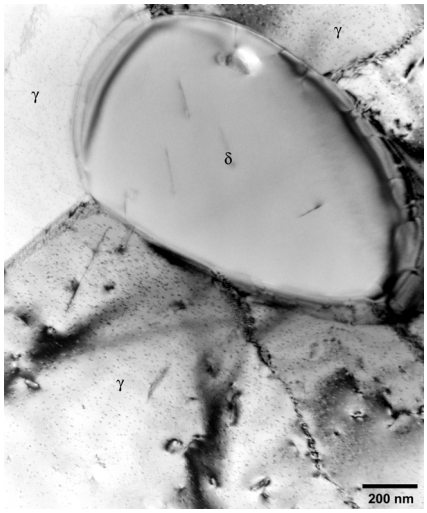

Figure 4. Image from a 5 vol.% δ ferrite weld showing a δ ferrite grain in an austenitic "matrix". The black "dots" in the austenite arise from strain contrast from helium bubbles. No black "dots" are visible in the δ ferrite.

The distribution of helium bubbles in the austenite in all of the weldments closely matched the helium bubble microstructure observed in the weld HAZs. That is, helium bubbles were observed within the grain interiors and not on the grain boundaries. The helium bubble distribution in the austenite is illustrated in Figure 5. These images are from austenite regions in a mixed wire weld on the 304L plate. Figure 5a is a high magnification image showing bubbles that nucleated in the interior of an austenite grain. The imaging conditions were such that many 2-3 nm sized bubbles (appearing as small "white" dots in this under-focused image) were visible. These bubbles likely formed by "homogeneous" nucleation at vacancies or vacancy clusters which are strong traps for helium in the matrix. In other austenite grains, helium bubbles were observed on dislocations (Fig. 5b). Dislocations are known to be potent heterogeneous nucleation sites for bubbles [5,6].

Interfaces play an important role in the fracture processes in tritium/helium-containing materials, so the austenite/austenite and austenite/ferrite boundaries in the weldments were investigated carefully. An interphase boundary is imaged in Fig. 6. Close examination of this and many other interfaces failed to detect bubbles in these areas. As mentioned above, the black "dots" in the austenite grain indicate the locations of helium bubbles.

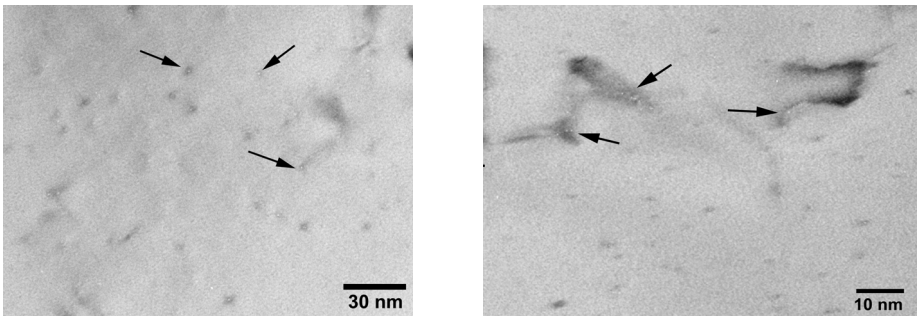

a. b.

Figure 5. Helium bubbles in the austenite phase. Bubbles have formed in the matrix (a) and on dislocations in (b).

Again, there are no black "dots" in the δ ferrite region in this image. Examination of the near-boundary region in this image also revealed a narrow region extending along the boundary region that is devoid of bubbles. Regions like this are termed bubble-free zones (BFZs) and were observed previously in another study [7]. BFZ formation is believed related to the reduction in the vacancy concentration in the near-boundary region which reduces the amount of trapped helium available to form bubbles.

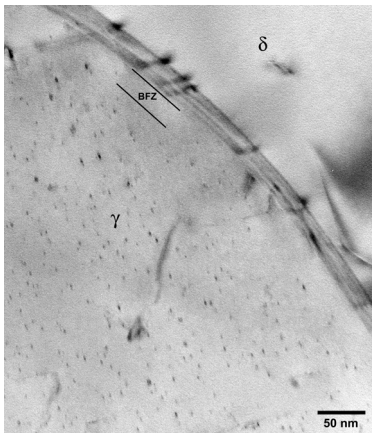

Figure 6. An image of an interface between the austenite and δ ferrite. Bubbles were not observed on these type boundaries. A bubble-free zone (BFZ) exists in the near boundary region.

DISCUSSION

The helium bubble distributions observed in the austenite phase were consistent with those observed in other studies at SRNL [1,3-5,7]. In these

studies, helium bubbles were observed commonly in the grain interiors, on dislocations, and sometimes on carbide/matrix interfaces and austenite/austenite grain boundaries. In the present study, helium bubbles were not observed in the δ ferrite phase. There are at least two possible reasons for this.

Firstly, it may simply be that there is less helium present in the δ ferrite to form bubbles. Unlike the fcc austenite phase (high hydrogen/tritium solubility and low diffusivity), the bcc ferrite phase is characterized by low tritium solubility and the rapid diffusion of tritium through the metal lattice. Therefore, the ferrite lattice tends to reject tritium and what is there diffuses out more rapidly before it decays to helium-3. Calculations show that pure α ferrite (also bcc) charged and aged using the sample conditions employed in the current study would contain about 13 appm helium [8]. This value is about 10 times less than the measured helium concentrations in the fully austenitic base materials. (Diffusivity/solubility differences may also explain the variability in the measured helium content of the welds as well as the drop-off in helium content in those welds containing high levels of ferrite.) As a result, the helium in the ferrite may be more widely dispersed over a large number of trap sites thus reducing the available helium in any one area to form a stable cluster or, at least, a cluster large enough to see in the TEM.

The second reason for not seeing helium bubbles in the δ ferrite may be related to the technique used to image them. Nanometer-sized helium bubbles are imaged in the TEM using an under/over-focusing technique [9]. In the under-focused condition bubbles appear brighter than the background, i.e., they look like voids, and in the over-focused condition bubbles appear as black dots and are darker imaging than the background. The imaging technique, however, is limited to resolving bubbles greater than about 0.7 nm in diameter. Below this size bubbles cannot be discerned from the background contrast in the image. Therefore, as alluded to above, bubbles (or maybe in fact, clusters of helium atoms) could have been present in the δ ferrite but were too small to be resolved with the TEM.

SUMMARY

The helium bubble distributions in fusion welds containing 4 to 33 volume percent δ ferrite and approximately 150 appm helium-3 were characterized. In the low δ ferrite welds, the microstructure was primarily austenite and discontinuous, skeletal δ ferrite. In welds with higher levels of δ ferrite the ferrite was more continuous and the austenite/ferrite interfaces more planar. In some areas of the highest δ ferrite weld, the ferrite was the matrix phase. Helium bubbles were observed in the austenite phase and not in the δ ferrite. The failure to observe bubbles in the δ ferrite was probably related to the limited solubility and the rapid diffusion of tritium in that phase resulting in a reduced amount of helium available to form bubbles of sufficient size to view

in the TEM. Bubbles in the austenite nucleated homogeneously in the grain interiors and on matrix dislocations. These results were consistent with previous studies of helium bubbles in austenitic stainless steels. Bubbles were not observed on the austenite/austenite or austenite/ferrite boundaries.

ACKNOWLEDGEMENTS

This document was prepared in conjunction with work accomplished under Contract No. DE-AC09-08SR22470 with the U.S. Department of Energy.

REFERENCES

1. Morgan, M. J. and Tosten, M. H., "Microstructure and Yield Strengths Effects on Hydrogen and Tritium-Exposed HERF Stainless Steels", Proc. 4th Int. Conf. on the Effects of Hydrogen on the Behavior of Materials, Moran, WY, 1990, pp. 447-58.

2. Morgan, M. J. and Lohmeier, D. A., "Threshold Stress Intensities and Crack Growth in Tritium-Exposed HERF Stainless Steels", Proc. 4th Int. Conf. on the Effects of Hydrogen on the Behavior of Materials, Moran WY, 1990, pp. 459-68.

3. Morgan M. J. and Tosten, M. H., "Tritium and Decay Helium Effects on the Fracture Toughness Properties of Types 316L, 304L, 21Cr-6Ni-9Mn Stainless Steels", Proc. 5th Int. Conf. on the Effects of Hydrogen on the Behavior of Materials, Moran, WY, 1996, pp. 873-82.

4. Tosten, M. H. and Morgan, M. J., "Microstructural Study of Fusion Welds in 304L and 21Cr-6Ni-9Mn Stainless Steels", WSRC-TR-2004-00456, WSRC, Aiken, SC.

5. Tosten, M. H and Morgan, M. J., "The Effects of Helium Bubble Microstructure on Ductility in Annealed and HERF 21Cr-6Ni-9Mn Stainless Steel", WSRC-RP-92-551, WSRC, Aiken, SC.

6. Robinson S. L., "Tritium and Helium Effects on Plastic Deformation in AISI 316 Stainless Steel", Mater. Sci. Eng., vol. 96, 1987, pp. 7-16.

7. Tosten, M. H. and Kestin, P. A., "Helium Bubble Distributions in Reactor Tank Repair Specimens - Part I.", WSRC-TR-91-141, WSRC, Aiken, SC.

8. Clark, E. A., WSRC, Unpublished research, 2005.

9. Rhüle, M. F., "Transmission Electron Microscopy of Radiation-Induced Defects", Proc. Int. Conf. on Radiation-Induced Voids in Metals, Albany, NY, 1972, pp. 255-91.